View metadata, citation and similar papers at core.ac.uk

brought to you by CORE

provided by NASA Technical Reports Server

LMSC-HEC TR F268618

Final Report

SSME LOX POST FLOW ANALYSIS / FLUID STRUCTURE INTERACTION

Volume I: Flow Analysis

June 1989

Contract NAS8-37361

Prepared for

NATIONAL AERONAUTICS AND SPACE ADMINISTRATION
GEORGE C. MARSHALL SPACE FLIGHT CENTER
MARSHALL SPACE FLIGHT CENTER, ALABAMA 35812

by

Roger W. Burke

Lockheed
Missiles & Space Company, Inc.
Huntsville Engineering Center
4800 Bradford Blvd., Huntsville, AL 35807

(NASA-CR-183677) SSME LOX POST FLOW ANALYSIS/FLUID STRUCTURE INTERACTION. VOLUME I: FLOW ANALYSIS Final Report (LMSC) 32 p CSCL 20D

N90-13715

G3/34 Unclas 0217277

Final Report

SSME LOX POST FLOW ANALYSIS / FLUID STRUCTURE INTERACTION

Volume I: Flow Analysis

June 1989

Contract NAS8-37361

Prepared for

NATIONAL AERONAUTICS AND SPACE ADMINISTRATION
GEORGE C. MARSHALL SPACE FLIGHT CENTER
MARSHALL SPACE FLIGHT CENTER, ALABAMA 35812

by

Roger W. Burke

Lockheed Missiles & Space Company, Inc.
Huntsville Engineering Center
Huntsville, AL 35807

FOREWORD

This final report presents the results of work performed by the Computational Mechanics Section of the Lockheed-Huntsville Engineering Center in fulfillment of the requirements of Contract NAS8-37361 for the National Aeronautics and Space Administration, George C. Marshall Space Flight Center. This document is submitted in two volumes:

I Flow Analysis

II Fluid Structure Interaction.

The work described in Volume II was performed by The Computational Mechanics Company, Inc., under subcontract to Lockheed.

The Contracting Officer's Technical Representative for this contract is G.A. Wilhold.

CONTENTS

LIST OF FIGURES

LIST OF FIGURES (Concluded)

1. INTRODUCTION

The realization of measures to improve the performance of the Space Shuttle is, to a large extent, dependent on an improved understanding of the fluid flow phenomena occurring in the main engine. Figure 1 presents the overall arrangement of the primary components of the Space Shuttle Main Engine (SSME). Hot gases flow from the high pressure hydrogen and oxygen turbopumps through the hot gas manifold transfer ducts and into the main injector. The flow then passes through a region of 600 circular cylinder shaped liquid oxygen (LOX) posts before exiting into the main combustion chamber. The flow in the LOX post core reaches a maximum Mach number of approximately 0.3, and can thus be considered as essentially incompressible.

The impingement of the hot gases from the transfer ducts onto the LOX posts (see Fig. 2) causes them to be subjected to severe thermal and gas dynamic loads, which in the past have resulted in the occasional breakage of some elements of the outer row of posts during test firings of the engine, particularly at higher power levels. Large velocities in the gap between the LOX posts may also be a contributing factor in causing dynamic stability problems. The deforming structural response of the posts to the pressure loading may likely affect the gas flowfield by producing a moving flowfield boundary, thereby creating a dynamically coupled unsteady fluid-structure system.

The objective of this study was to investigate the three-dimensional, turbulent flow around a simplified SSME LOX post array using an existing Reynolds averaged Navier-Stokes flow solver and a suitable turbulence model to parameterize the turbulent shear stresses. Numerical computations were performed to analyze the effect on the flowfield of varying the spacing between the LOX posts, which were modeled as rigid, three-dimensional circular cylinders. In addition, a finite element theory for treating the fluid/structure interaction between the posts and the hot gas environment was developed by Dr. Oden and is submitted as Volume II.

The methodology used in the computations is described in Section 2. Results are presented in Section 3 and concluding remarks in Section 4.

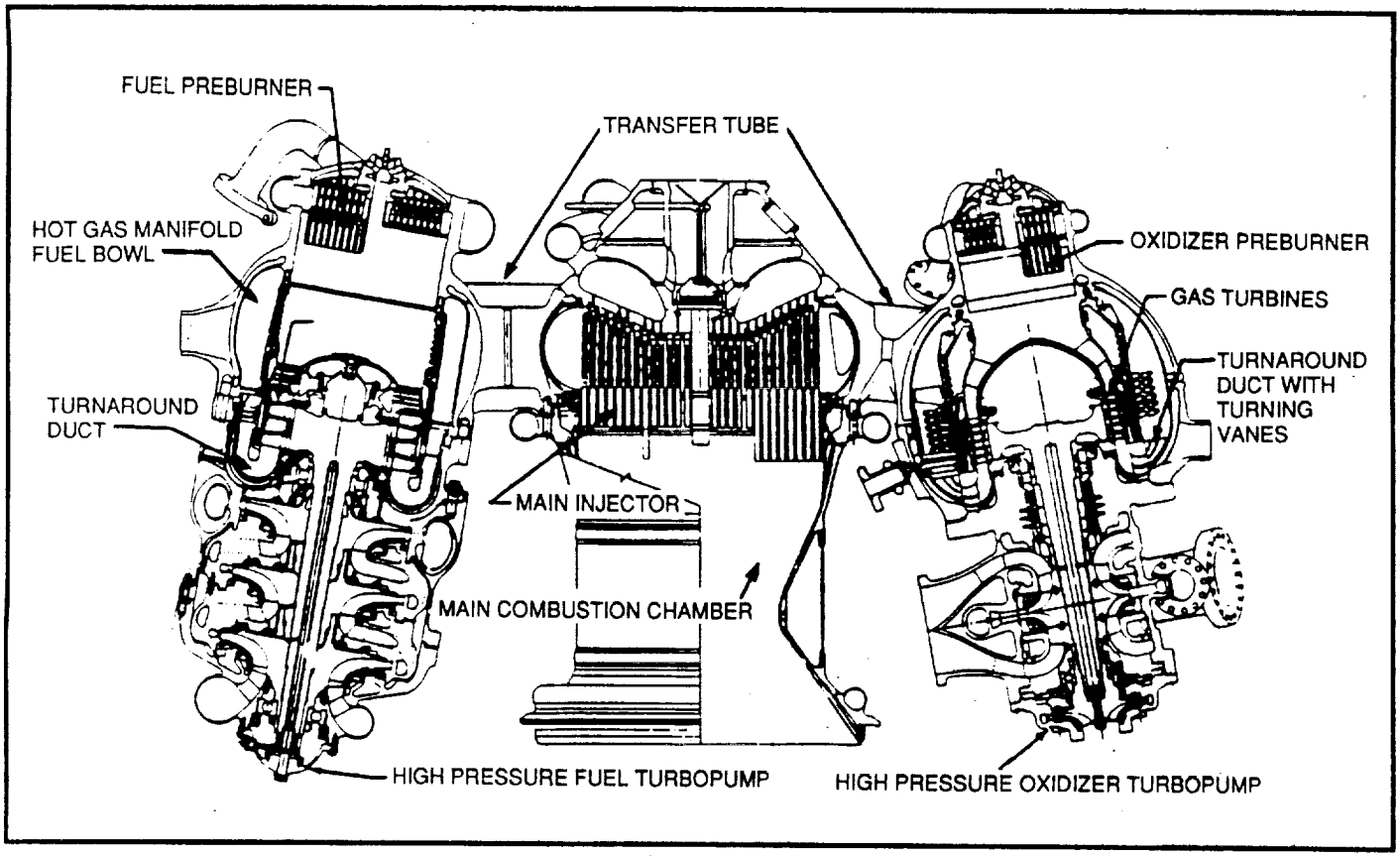

Figure 1 Space Shuttle Main Engine Powerhead Arrangement

ORIGINAL PAGE
BLACK AND WHITE PHOTOGRAPH

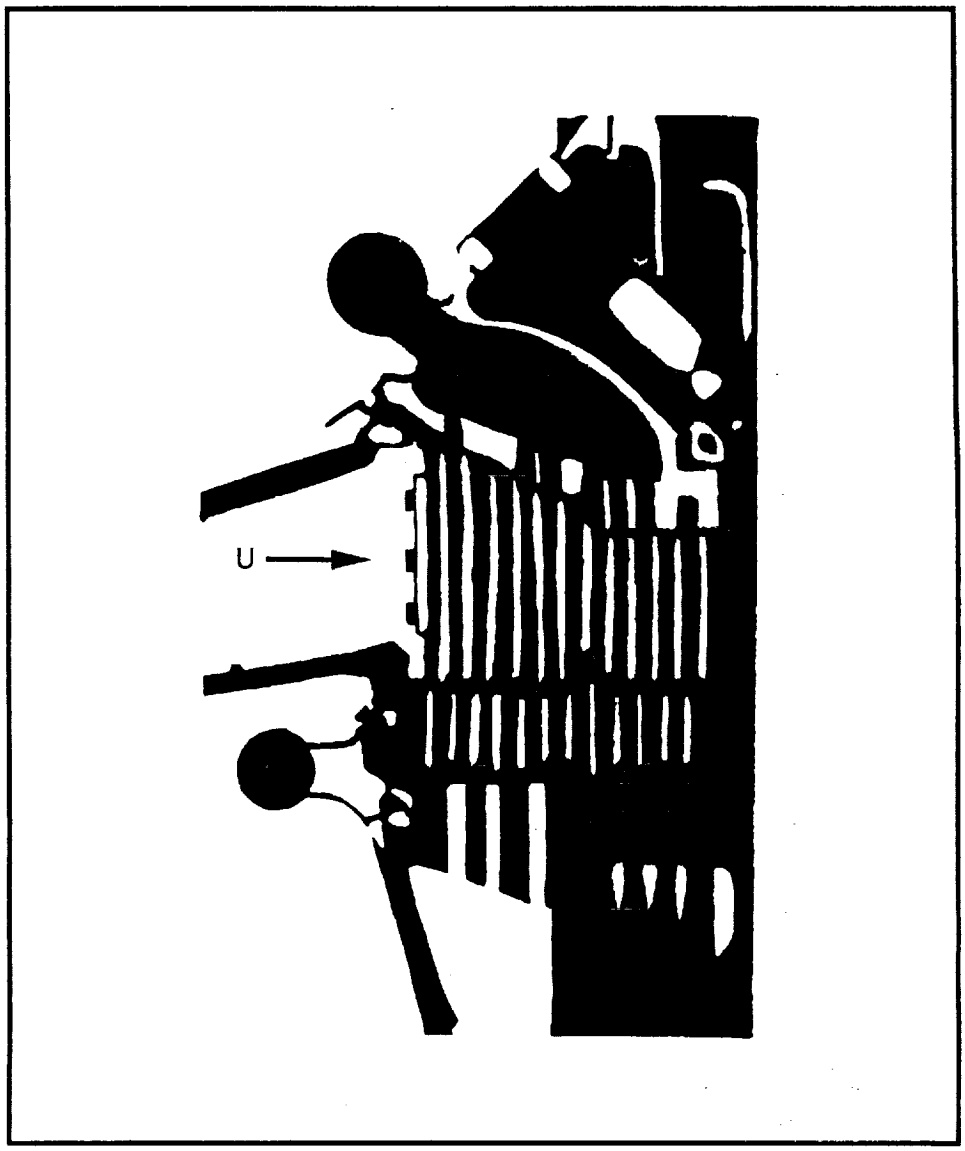

Figure 2 Transfer Duct and LOX Post Core

2. APPROACH

2.1 BACKGROUND AND SCOPE OF WORK

Two-dimensional flow around single cylinders has been the subject of extensive investigation, both experimental and computational. In contrast, the flow around multiple cylinders has received somewhat less attention. Numerical predictions of two-dimensional laminar flow past an array of cylinders have been made by Cerutti et al. (Ref. 1) and Antonopoulos and Gosman (Ref. 2), among others. Typically, these studies focus on analyzing the flow in tube banks, such as occur in heat exchangers. In this context, Antonopoulos (Ref. 3) has applied a two equation "k-ϵ" turbulence model to the problem of turbulent inclined flow in rod bundles.

Numerical studies aimed at analyzing the flow around LOX post arrays have been conducted by Rogers et al. (Ref. 4) and Williams (Ref. 5). Rogers calculated the laminar flow past multiple posts mounted perpendicularly between channel end walls. Only one-half of the channel was included in the computations, with symmetry boundary conditions being applied at the mid-height of the channel. Periodic boundary conditions were applied at the side boundaries, thus representing an infinite array of posts. Calculations were also performed for flow around two staggered arrays of posts, with one row behind the other. Williams (Ref. 5) used a multiblock procedure to analyze the three-dimensional laminar flow around multiple posts. The effect of protective shields placed on the posts to protect them from loose debris was investigated by modeling the posts as closely spaced elliptical cylinders. The effect of a secondary row of posts was also considered.

Extending the earlier work on flow around LOX post arrays, this study considers the turbulent flow around multiple posts aligned with their axes normal to the direction of oncoming flow. Following the approach of Rogers (Ref. 4), the posts are taken as being attached at both ends to flat plates a distance (h) apart. The coordinate system (see Fig. 3) is oriented so that x is in the streamwise direction, y in the cross-stream direction, and z normal to the flat plate. The origin of the coordinate system is on the flat plate at the leading edge of the post. The nondimensional diameter (d) of the posts is equal to one, with the distance between the flat plates equal to 8d. The Reynolds number, based on cylinder diameter, is $1.0 \cdot 10^6$.

The computational domain extends from one flat plate to a vertical height (in the z direction) of h/2, at which symmetry boundary conditions are imposed. Only one post is considered, with periodic boundary conditions applied at $y=\pm$ s/2 (see Fig. 3), thereby representing an infinite array of posts in the cross-stream direction having a

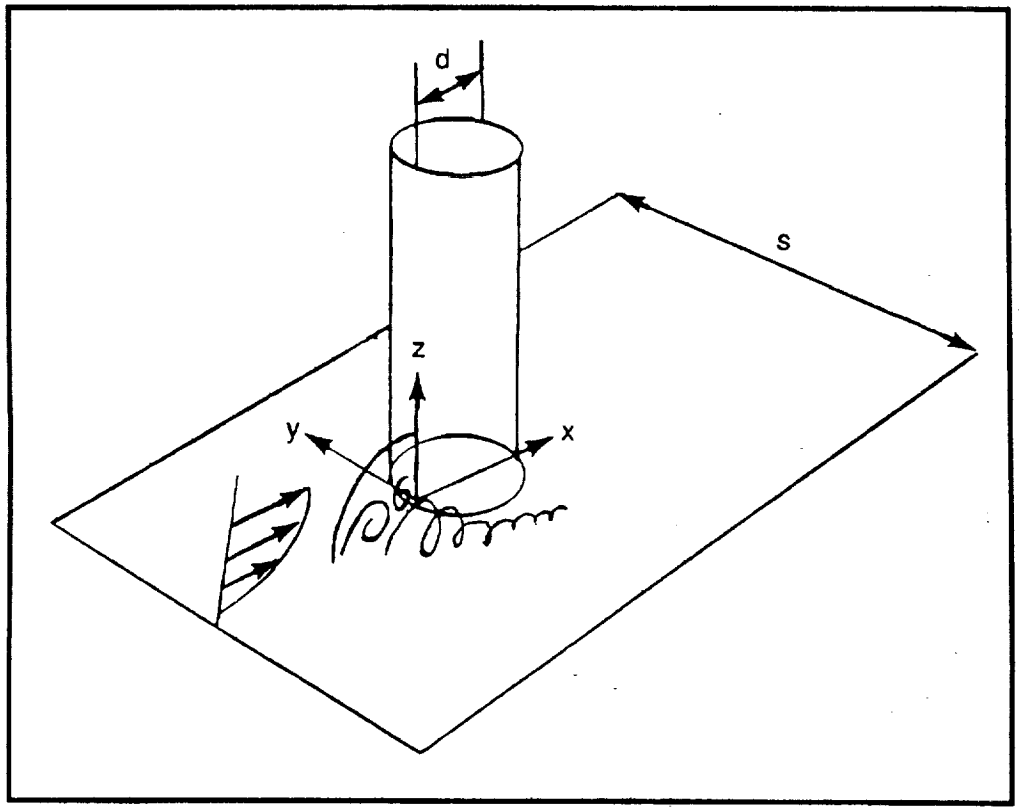

Figure 3 Post on Flat Plate

center-to-center spacing of "s." The variation of the flowfield parameters as a function of post spacing is investigated by varying the width of the side boundaries.

Computations were also performed for a single post mounted on a flat plate and the results compared to wind tunnel experiments of Baker (Ref. 6) for the size of the horseshoe vortex system and pressure distribution on the flat plate ahead of the cylinder.

2.2 FLOW SOLVER

Computations for incompressible flow were performed using the INS3D code, which was developed by Kwak et al. (Ref. 7). This is an implicit, finite difference code cast in general curvilinear coordinates for solving the three-dimensional steady state Reynolds averaged Navier-Stokes equations using a Briley-McDonald (Ref. 8)/ Warming-Beam (Ref. 9) approximate factorization method. The pressure is handled using a pseudocompressibility approach, first proposed by Chorin (Ref.10). Reference 7 provides a detailed description of the INS3D methodology.

2.3 TURBULENCE MODEL

The turbulent transport phenomena occurring in complex flows such as those around a cylinder mounted on a flat plate are complex and not well understood. One of the major difficulties with this type of configuration is accounting for the influence of more than one surface on the turbulent length and velocity scales. A common turbulence modeling approach for geometries having more than one surface is to use a two equation technique, such as the "k–ϵ" approach, which does not require any a priori specification of the turbulent scales. Before pursuing this relatively more complex, and computationally expensive, approach it was decided to investigate the use of a relatively simpler, zero-equation model.

In this study the turbulent shear stresses are parameterized using a Prandtl mixing-length model in which the turbulent eddy viscosity (μ_t) is taken as

$$\mu_t = \varrho l^2 |\omega| \tag{1}$$

where ϱ is the density, $|\omega|$ is the absolute vorticity, and (l) is the mixing length.

The mixing-length (l) is taken after a study by Patankar (Ref. 11) for flow in internally finned tubes. In this approach, l is given by

$$1/l = \sum_{i=1}^{s} 1/(kn_iD_i) \tag{2}$$

where s is the number of surfaces in the problem, k is Von Karman's constant, n_i is the distance from the ith surface, and D_i is the Van Driest damping factor associated with the ith surface. Thus, for instance, for the flow around a post mounted on a flat plate, s=2 and the mixing length at any point in the fluid medium is given by

$$1/l = 1/kn_1D_1 + 1/kn_2D_2 \tag{3}$$

where n_1 is the distance from the flat plate. Upstream of the post trailing edge (x/d< 1.0), n_2 is the distance from the cylinder surface; downstream of the post trailing edge (x/d > 1.0), n_2 is the distance from the wake centerline.

This approach for computing the mixing length has the advantage of easily accounting for the influence of more than one surface on the turbulent length scale. The nearer a point is to the ith surface, the greater the influence of that point on the mixing length. In the limit as n_i goes to zero near the ith surface, the mixing length approaches kn_iD_i, which is the standard mixing length expression for a single surface.

This formulation for the turbulent eddy viscosity outlined here has been used in earlier work (Ref.12) for flow around a wing mounted on a flat plate, and was found to give generally good agreement with experimental wind tunnel data (Ref. 13) for the size of the horseshoe vortex formed at the wing/flat plate junction as well as for the pressure distribution on the flat plate and for mean velocities.

2.4 BOUNDARY CONDITIONS

Explicit boundary conditions are used in the calculations. No slip conditions are applied on the solid surfaces. The pressure on these surfaces is determined by specifying a normal zero pressure gradient, i.e.,

$$\frac{\delta p}{\delta n} = 0.0 \tag{4}$$

where n represents the direction normal to the surface.

Conditions for the downstream boundary are the most difficult to provide and require careful specification to avoid numerical instabilities and non-convergence. The downstream values of pressure and velocity are updated in the manner prescribed by Chang et al. (Ref. 14). In this approach, a second-order upwind extrapolation is first used to update the velocities normal to the exit plane. Next, these updated velocities are mass-weighted to conserve the inlet mass flux. A new pressure corresponding to these mass-weighted velocities is then determined to ensure conservation of momentum flux at the outflow.

Periodic boundary conditions are applied at the side boundaries of the computational domain to simulate an infinite row of posts in the cross-stream direction. At the inlet the static pressure and velocity profile are specified and held fixed. The velocity profile is derived from a one-seventh power law formulation given by

$$U/U_o = (z/bl)^{1/7} \tag{5}$$

where bl is the height of the boundary layer and U_o is the free stream reference velocity.

2.5 GRID

The grids used in the computations were generated using the Lockheed-Huntsville algebraic grid generator. The three-dimensional grid around a post was created by first generating a two-dimensional C-grid and then stacking the grid in the vertical direction

normal to the flat plate, using a suitable stretching routine. The grid for the single post consisted of 95 points along the body, 41 away from the body, and 41 away from the flat plate (see Figs. 4 and 5). The multiple post grid (Figs. 6 and 7) also had 95 points along the body, with 31 points away from the post, and 54 points away from the flat plate. In order to resolve the near wall gradients, the grids were stretched away from both the post and the flat plate.

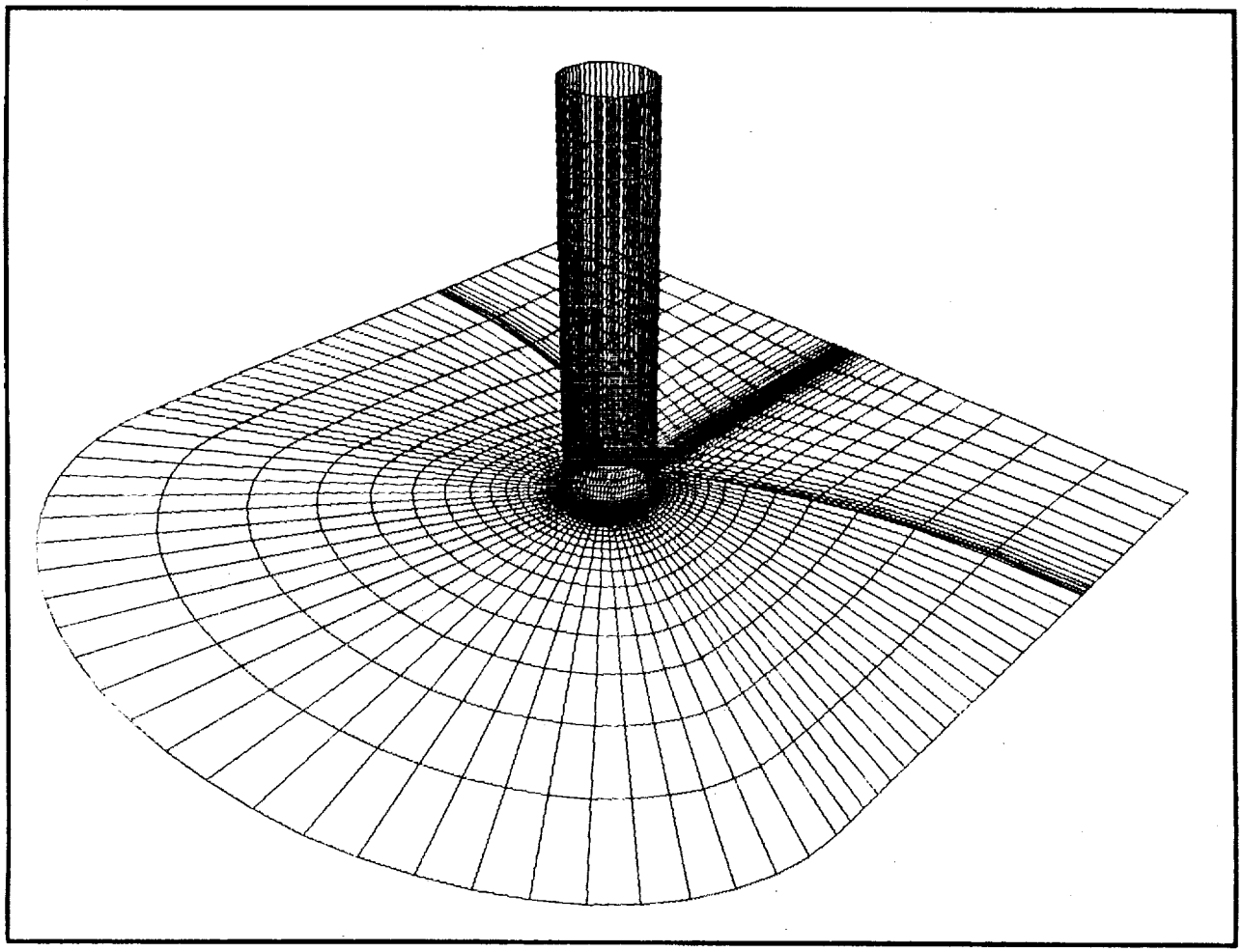

Figure 4 Side View of Mesh System for Single Post on Flat Plate

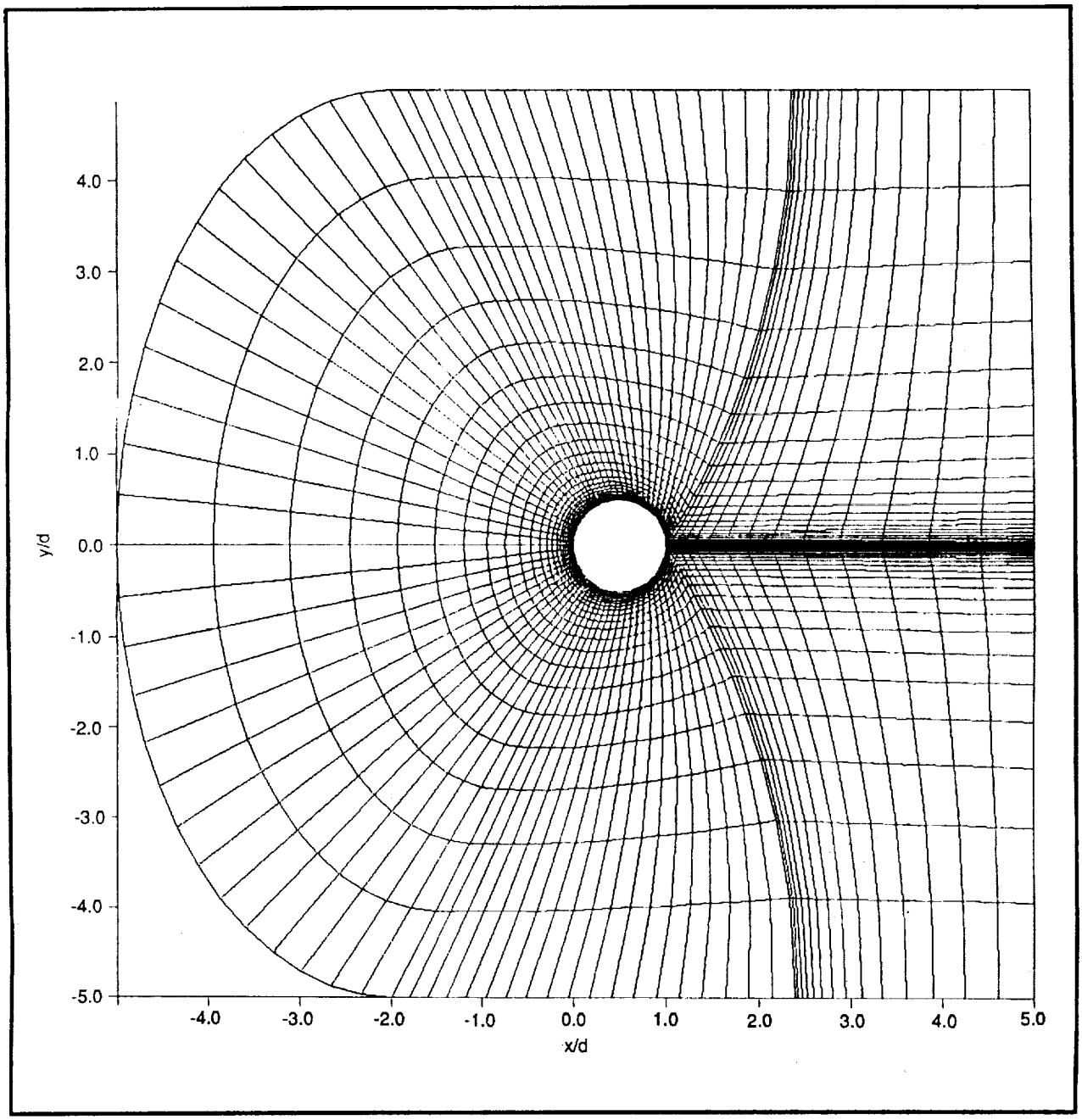

Figure 5 Top View of Mesh System for Single Post on Flat Plate

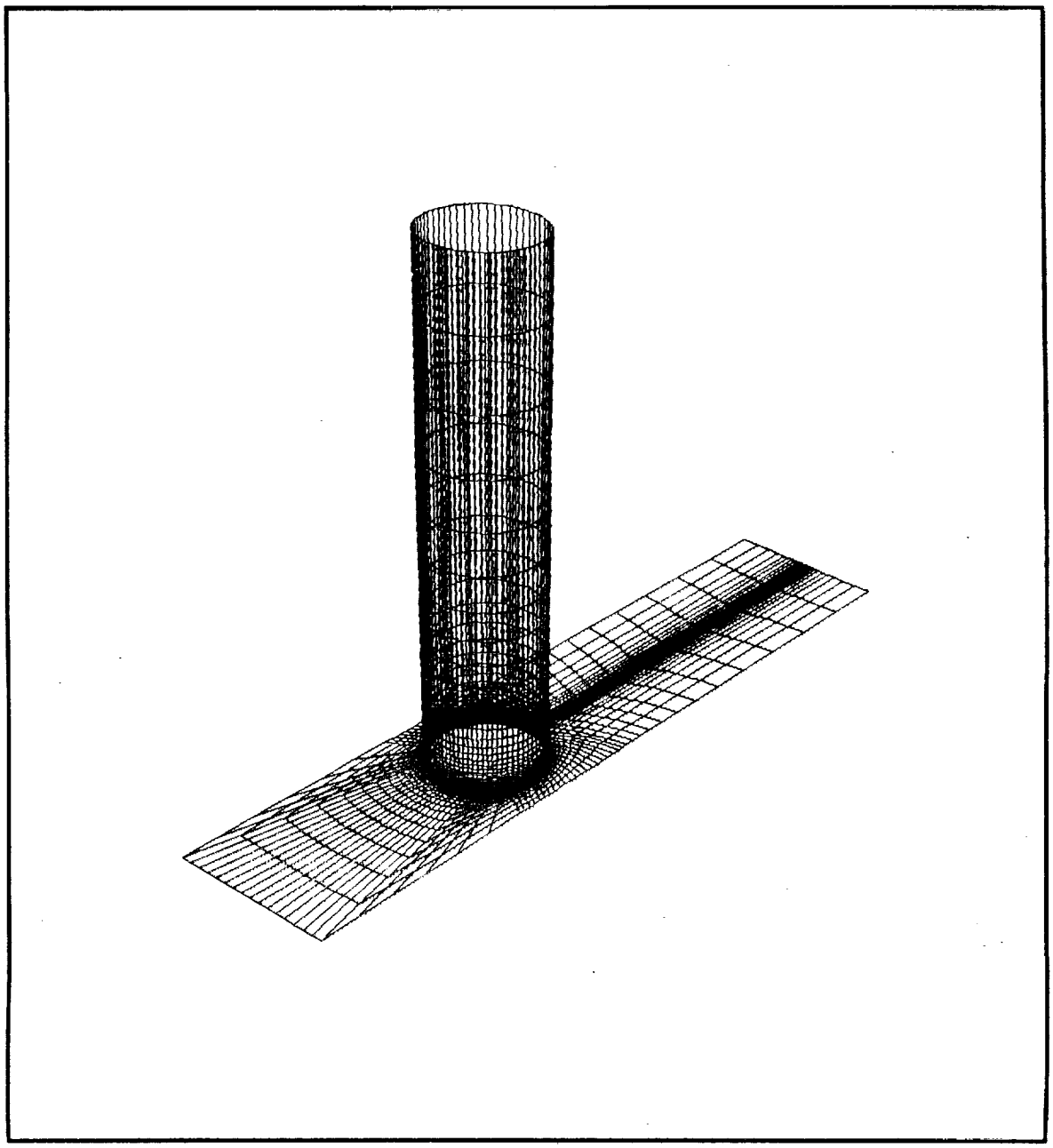

Figure 6 Side View of Mesh System for Multiple Posts

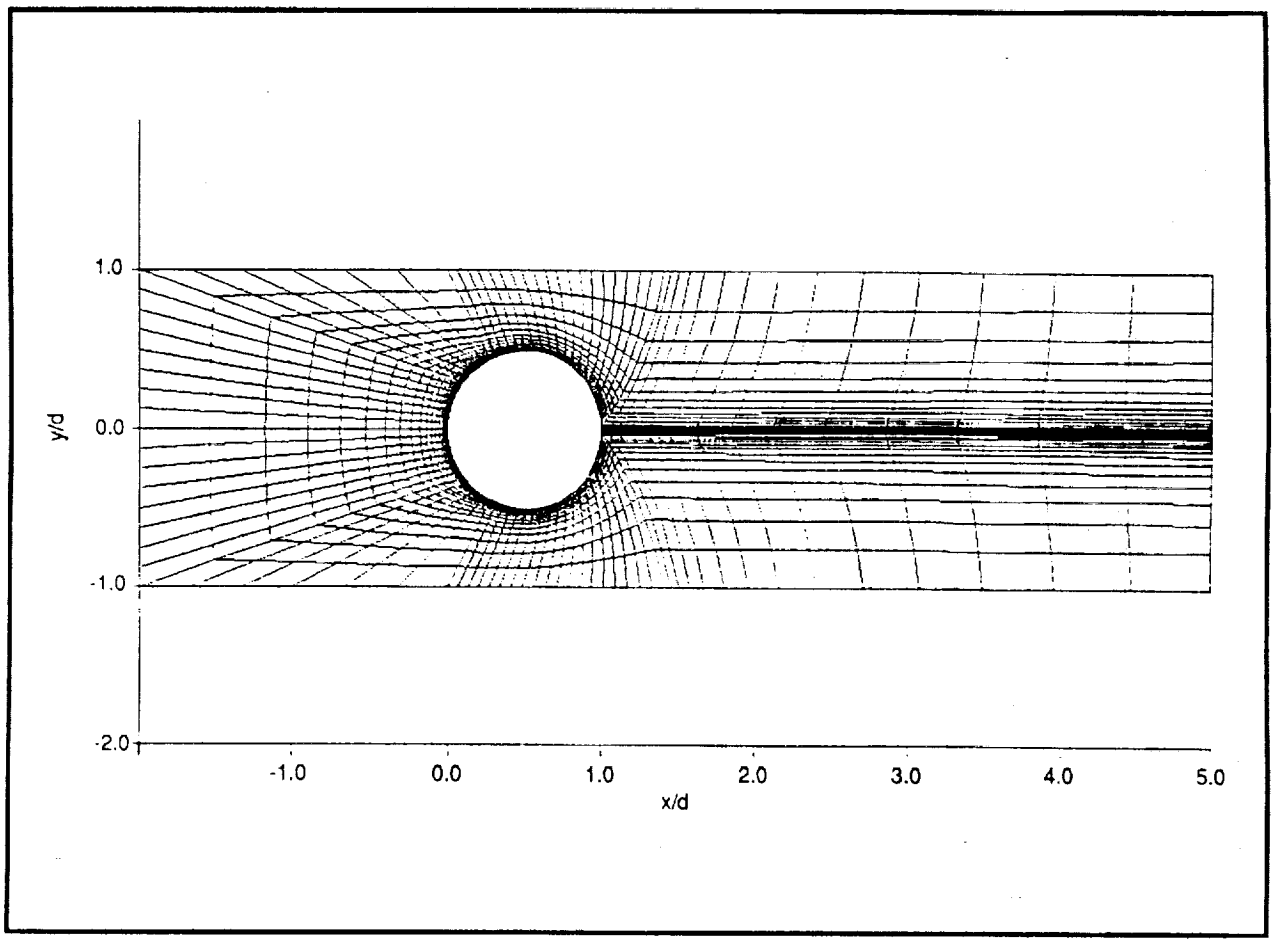

Figure 7 Top View of Mesh System for Multiple Posts

3. RESULTS

This section presents numerical calculations for turbulent flow around a single post mounted between two channel end walls, with the computed results being compared against the experimental wind tunnel data of Baker (Ref. 6). Results are also presented for multiple posts between two channel end walls. The height of the channel for both the single and multiple post cases is eight post diameters. The computations extend from the flat plate to mid-channel height, where symmetry boundary conditions are applied. Periodic boundary conditions are applied at the side boundaries (see Fig. 3) to represent an infinite array of posts. The distance between the side boundaries was varied to simulate different post spacings. Five cases were considered, with center to center distance between posts (s) of 1.5, 2.0, 2.5, 3.0, and 4.0 diameters.

3.1 SINGLE POST ON FLAT PLATE

Calculations were performed for a single post between two flat plates, with comparisons being made against the experimental wind tunnel data of Baker (Ref. 6). Flow in which a blunt obstruction is placed in the path of an oncoming boundary layer, such as a post mounted or a flat plate, is typically referred to as wing/body or junction flow. A region of adverse pressure gradient exists upstream of the obstruction leading edge, causing the oncoming boundary layer to undergo a three-dimensional separation. The separated boundary layer rolls up to form a vortex system upstream of the obstruction. This vortex system is swept around the base of the obstruction in the characteristic shape that gives rise to its name: the horseshoe vortex system.

Figure 8 shows an idealization of the limiting streamlines of a horseshoe vortex system at the base of a cylinder mounted on a flat plate. Particles originating very near the cylinder surface converge toward the primary separation line, which acts as a dividing streamline between the separated and mainstream regions. Upstream of the cylinder along the plane of symmetry the streamlines converge toward the saddle point of separation (xs), which is the location of the separation of the oncoming boundary layer.

Through the use of dimensional analysis, Baker concluded that the dependent dimensionless parameters governing wing/body type flows would generally be a function of the Reynolds number and d/δ, where δ is the boundary layer displacement thickness in the approaching boundary layer.

Figure 9 compares the experimental and computed oil film flow visualizations of the horseshoe vortex at the cylinder/flat plate junction for R_e=1.1·105 and d/δ=11.3.

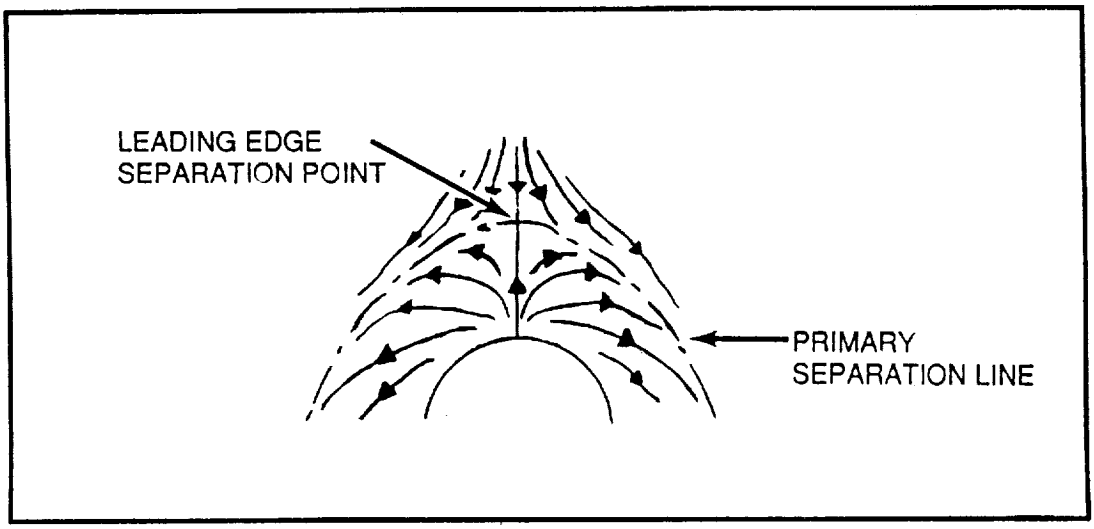

Figure 8 Schematic of Oil Film Flow Pattern

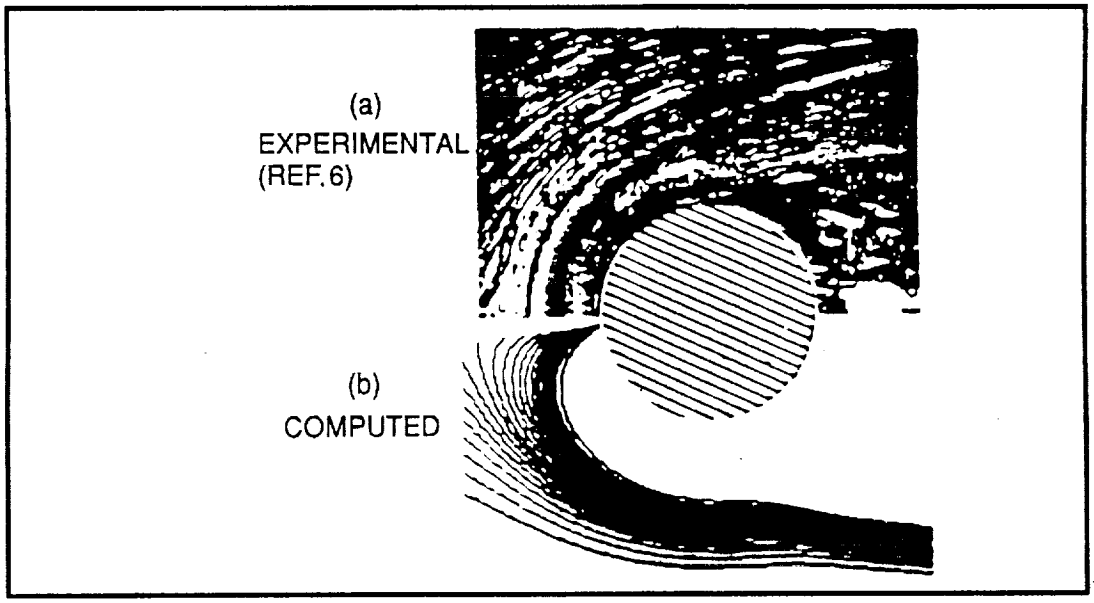

Figure 9 Oil Flow Lines at the Cylinder/Flat Plate Junction

The agreement is seen to be quite good, in terms of both the size and the shape of the horseshoe vortex system, as well as the location of the leading edge separation point (xs).

Particle paths on the symmetry plane ahead of the cylinder are shown in Fig. 10. As the particles approach the cylinder surface they divert downward, forming a

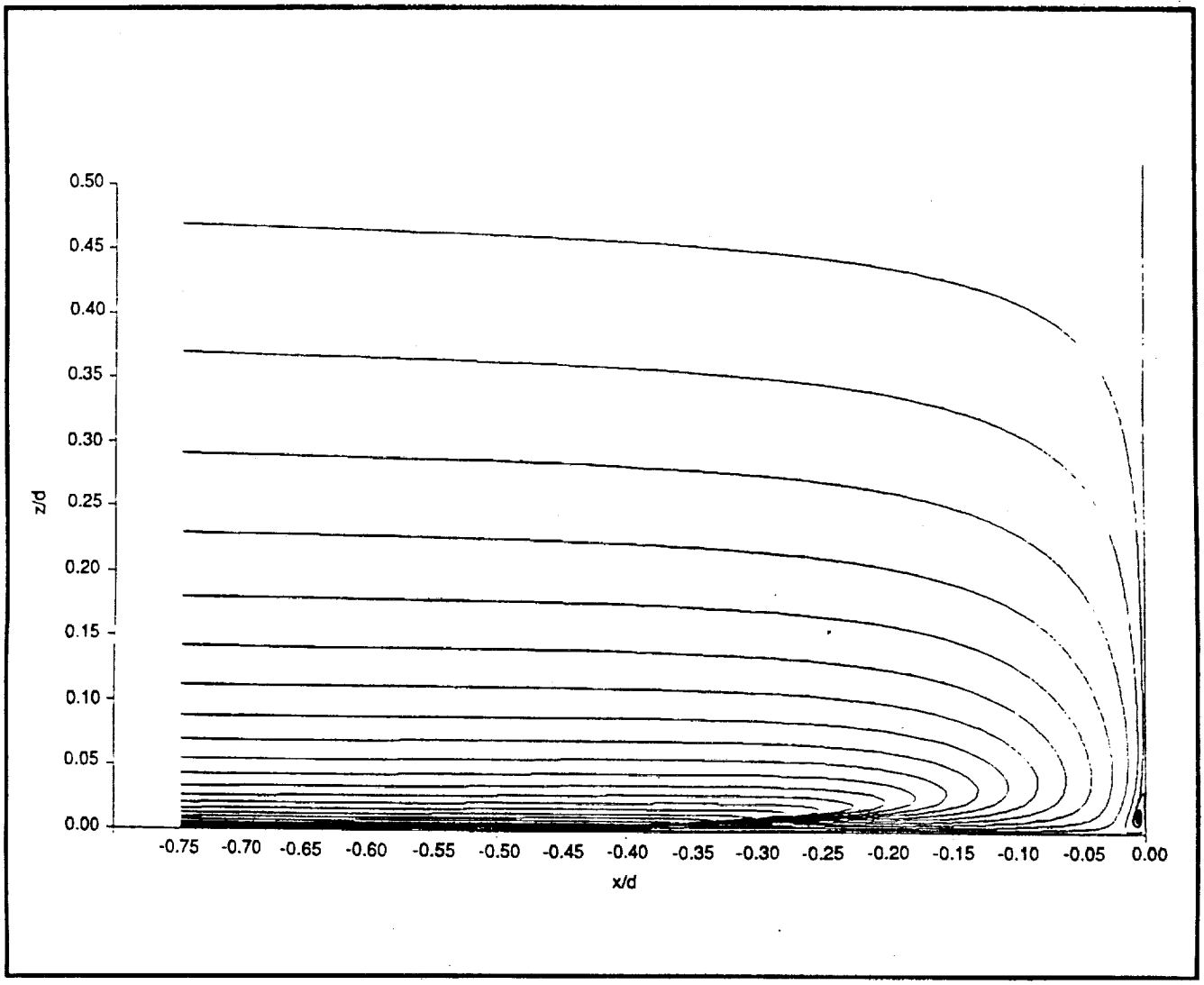

Figure 10 Particle Paths on the Symmetry Plane Ahead of Single Post (R_e=1.1·105, d/δ=11.3)

recirculating vortex region. A small counter-rotating vortex is visible in the very near-wall junction region. This counter-rotating vortex system is more clearly seen in the velocity vectors of Fig. 11.

In addition to oil film flow visualization, Baker (Ref. 6) also measured the pressure coefficient (C_p) on the flat plate ahead of the cylinder along the symmetry plane for various values of R_e and d/δ.

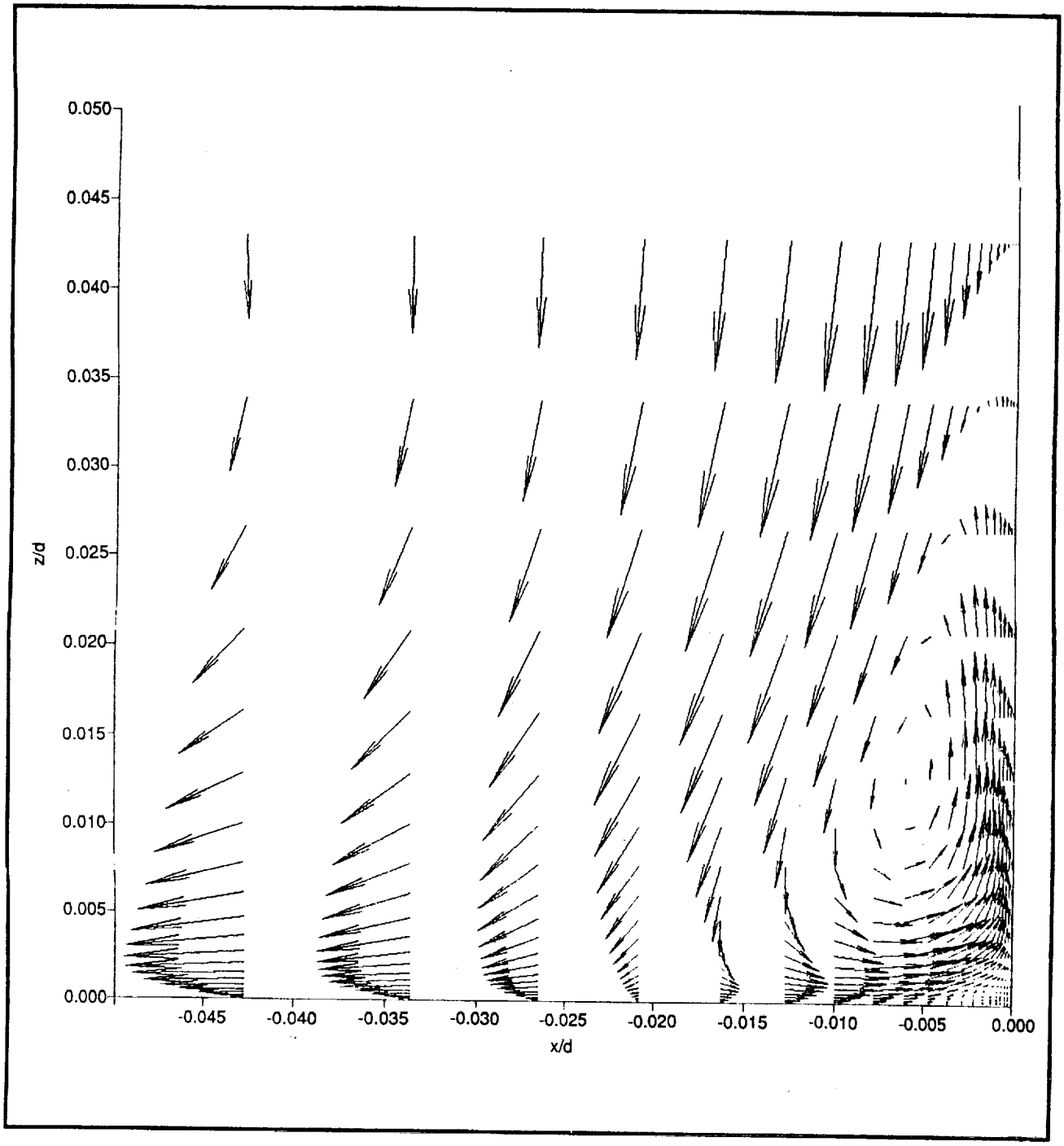

Figure 11 Counter-Rotating Inner Vortex at Symmetry Plane for Single Post (R_e=1.1·105, d/δ=11.3)

Figure 12 shows experimental values of pressure on the flat plate ahead of the cylinder on the plane of symmetry (y=0.0) for a Reynolds number between 5200 and 81000, and d/δ between 7.6 and 9.8. Also shown in Fig. 12 are the computed results for R_e=1.1·105 and d/δ=11.3. The agreement is seen to be generally satisfactory. A steep adverse pressure gradient is observed in both the experimental and computed results ahead of the post leading edge. This adverse pressure gradient is largely responsible for the skewing of the vortex lines in the oncoming boundary layer and the resultant formation of the horseshoe vortex system.

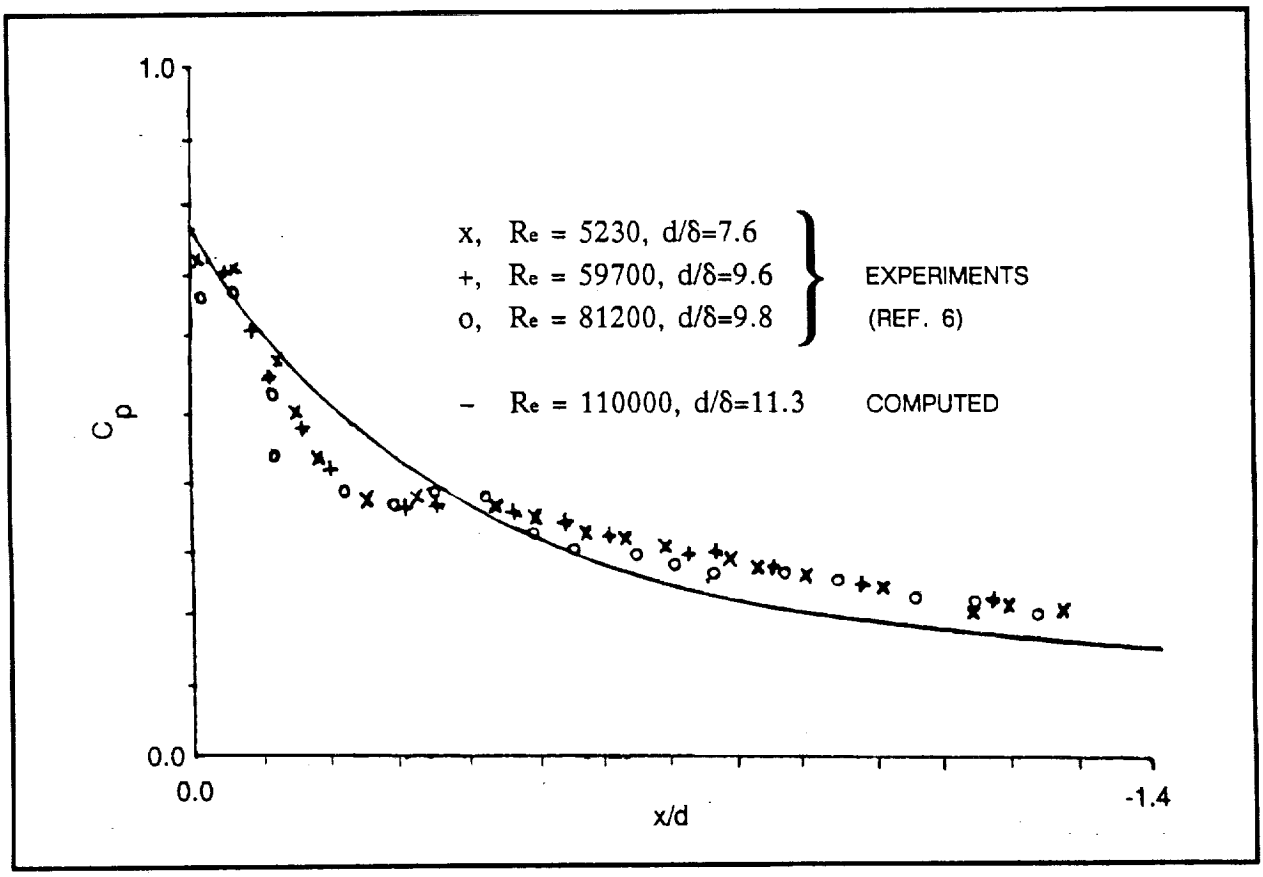

Figure 12 Pressure Distribution on Flat Plate

3.2 MULTIPLE POSTS

Computations were performed for an equally spaced array of posts in the plane normal to the oncoming flow. As discussed previously, the posts are taken as being attached at both ends to flat plates. Only one post was considered, with periodic boundary conditions being applied at the side boundaries (y = ±0.5s) in order to

represent an infinite row of posts with center to center spacing of s. The effect of strut spacing on the flow was investigated by varying the width of the side boundaries. Five cases were considered, corresponding to s/d = 1.5, 2.0, 2.5, 3.0, and 4.0. The Reynolds number, based on post diameter, was $1.0 \cdot 10^6$; d/δ was 35.7.

Figure 13 shows the simulated oil film flow visualization of the horseshoe vortex on the post/flat plate juncture region for the case with a post spacing (s) of 1.5d. For comparison, the oil flow lines for a single post are also shown in Fig. 13. The leading edge separation point (xs) occurs approximately 0.40 post diameters ahead of the cylinder leading edge for both the multiple and single post.

Figure 14 shows the particle paths on the symmetry plane ahead of the post for s=1.5d. Similar to the results for the single post case, a large vortex region is observed upstream of the post leading edge, with a smaller counter-rotating vortex system in the post/flat plate junction region.

Figure 15 shows the particle paths for particles released near the flat plate ahead of the cylinder for two post spacings corresponding to s/d=1.5 and s/d= 4.0. In both cases the particles spiral upward slightly behind the post. This spiraling phenomenon was also observed in the laminar calculations of flow around a single post (Ref. 15), as well as in the studies of Rogers (Ref. 4) and Williams (Ref. 5) for laminar flow around multiple posts.

The variation of the mass weighted average total pressure distribution (P_{tot}) with streamwise distance for various post spacings is shown in Fig. 16. P_{tot} is calculated as

$$P_{tot} = \frac{\int (P + 0.5U_{tot}^2) q dA}{\int q dA} \tag{6}$$

where P is the static pressure, U_{tot} the total velocity, q the mass flux, and dA the incremental area. At the inlet, where the velocity profile and static pressure are held fixed, the total pressure remains the same for all five cases. The drop in total pressure across the post varies inversely with post spacing. This relationship is believed due to the greater amount of separation occurring at the smaller post spacings. Downstream of the post trailing edge the drop in total pressure is significantly reduced. This trend is observed in all five cases.

Figure 17 shows profiles of streamwise velocity against distance from the flat plate at the point x/d=0.5, y/s=0.5, i.e., on the plane equidistant between adjacent posts.

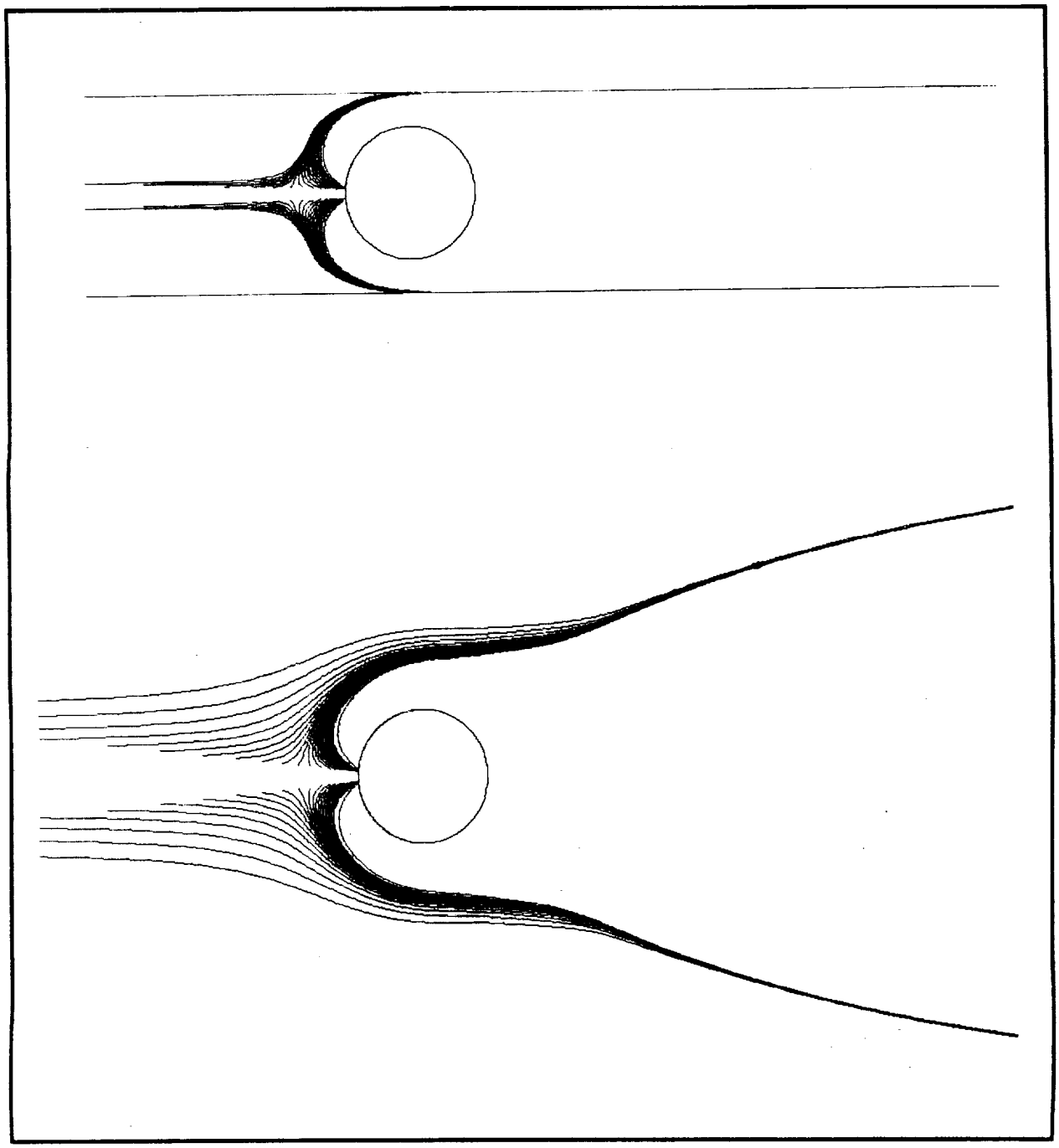

Figure 13 Oil Flow Lines for Multiple Posts with s=1.5d (Top), and for Single Post

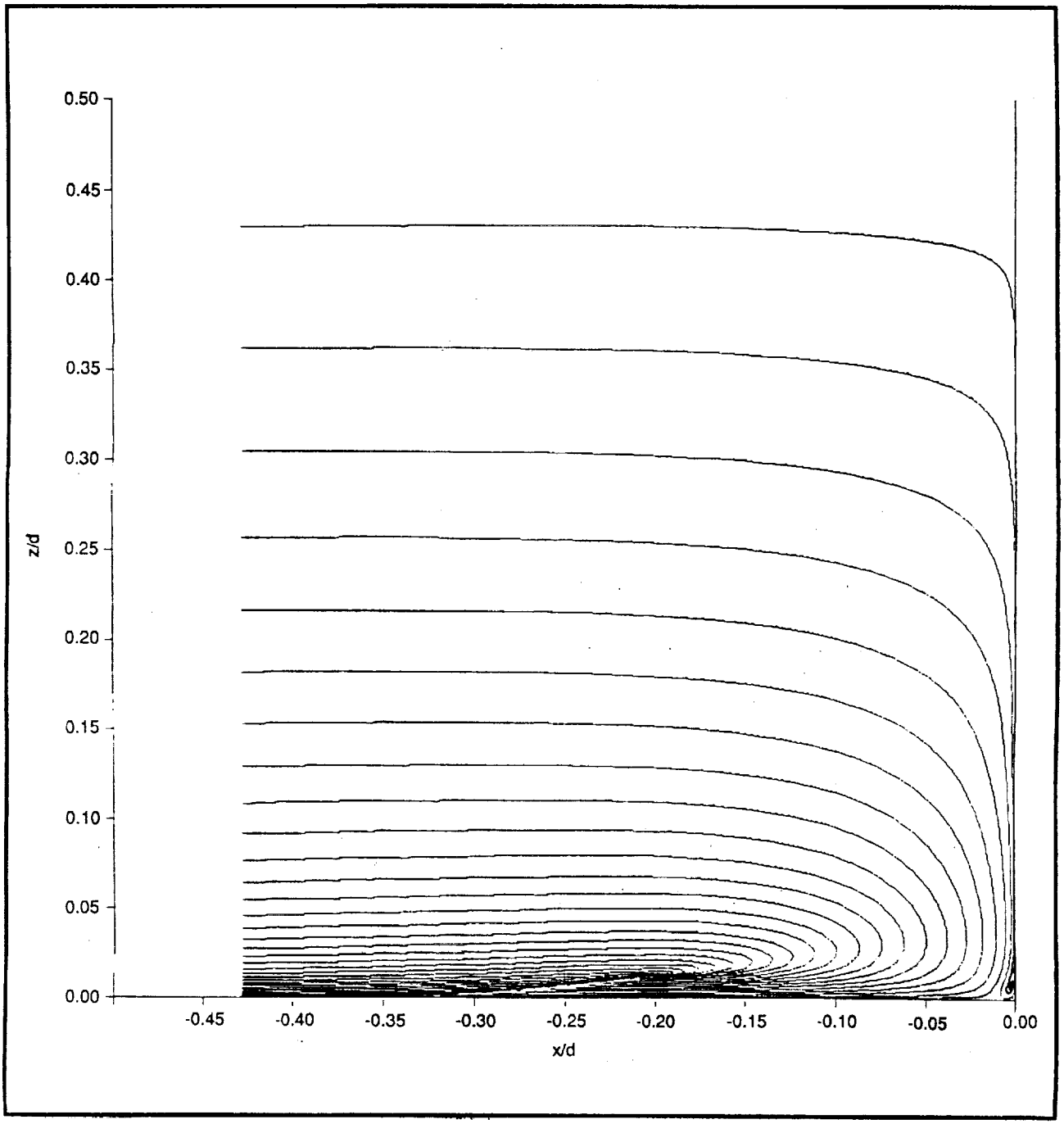

Figure 14 Particle Paths on Symmetry Plane Ahead of Strut for s=1.5d

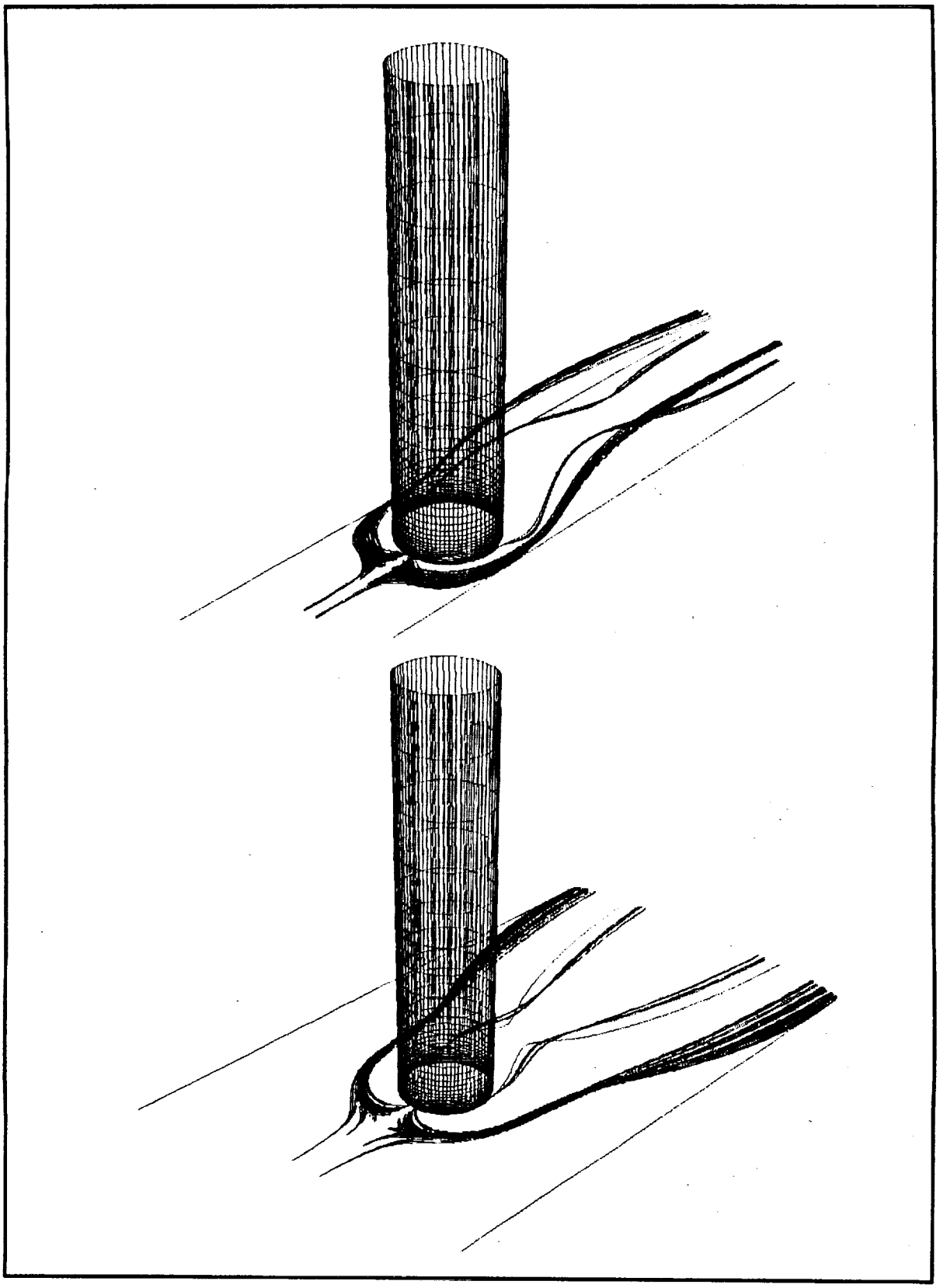

Figure 15 Particle Paths for s=1.5d (Top) and s=4.5d (Bottom)

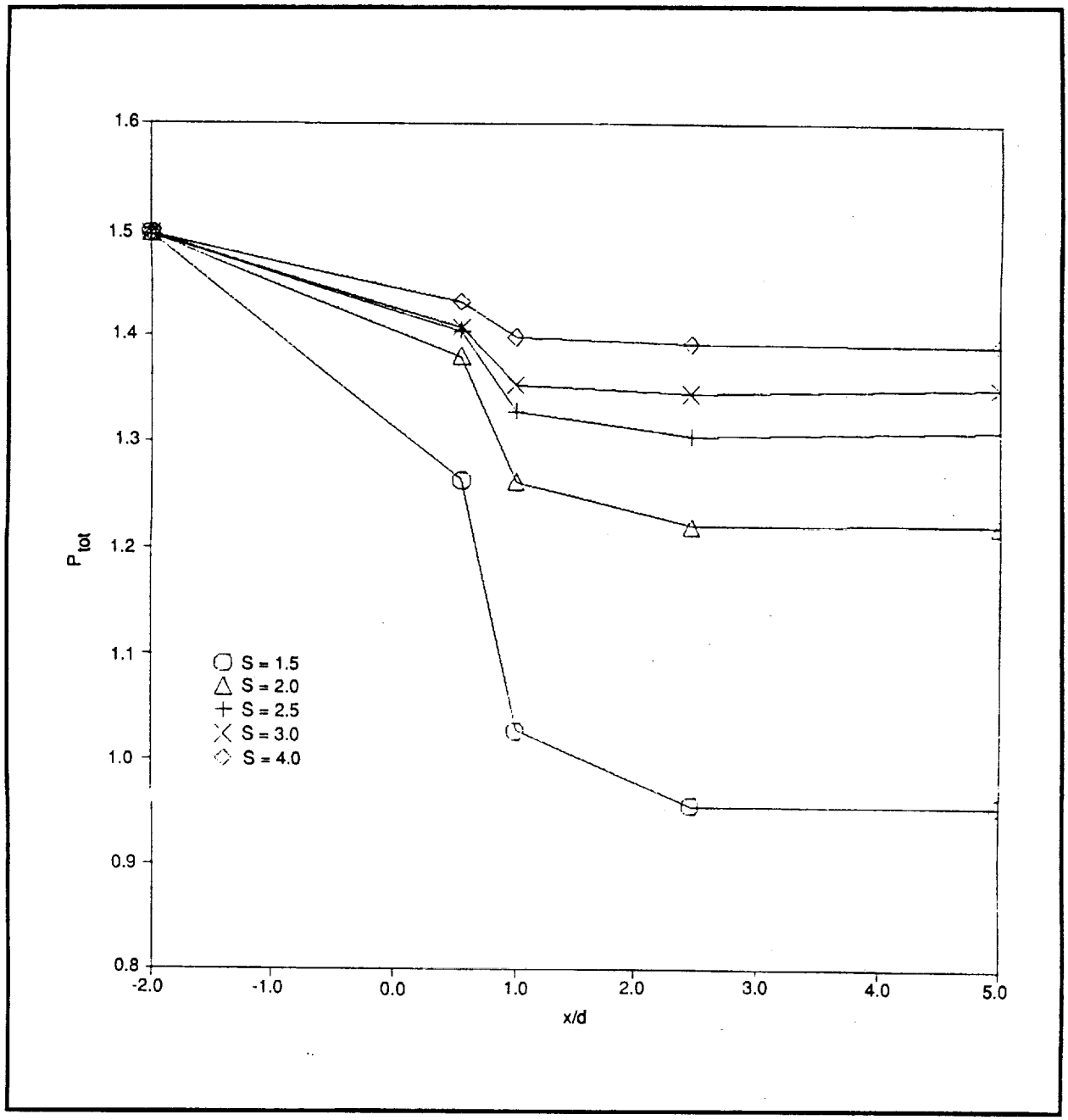

Figure 16 Variation of Total Pressure with Streamwise Distance

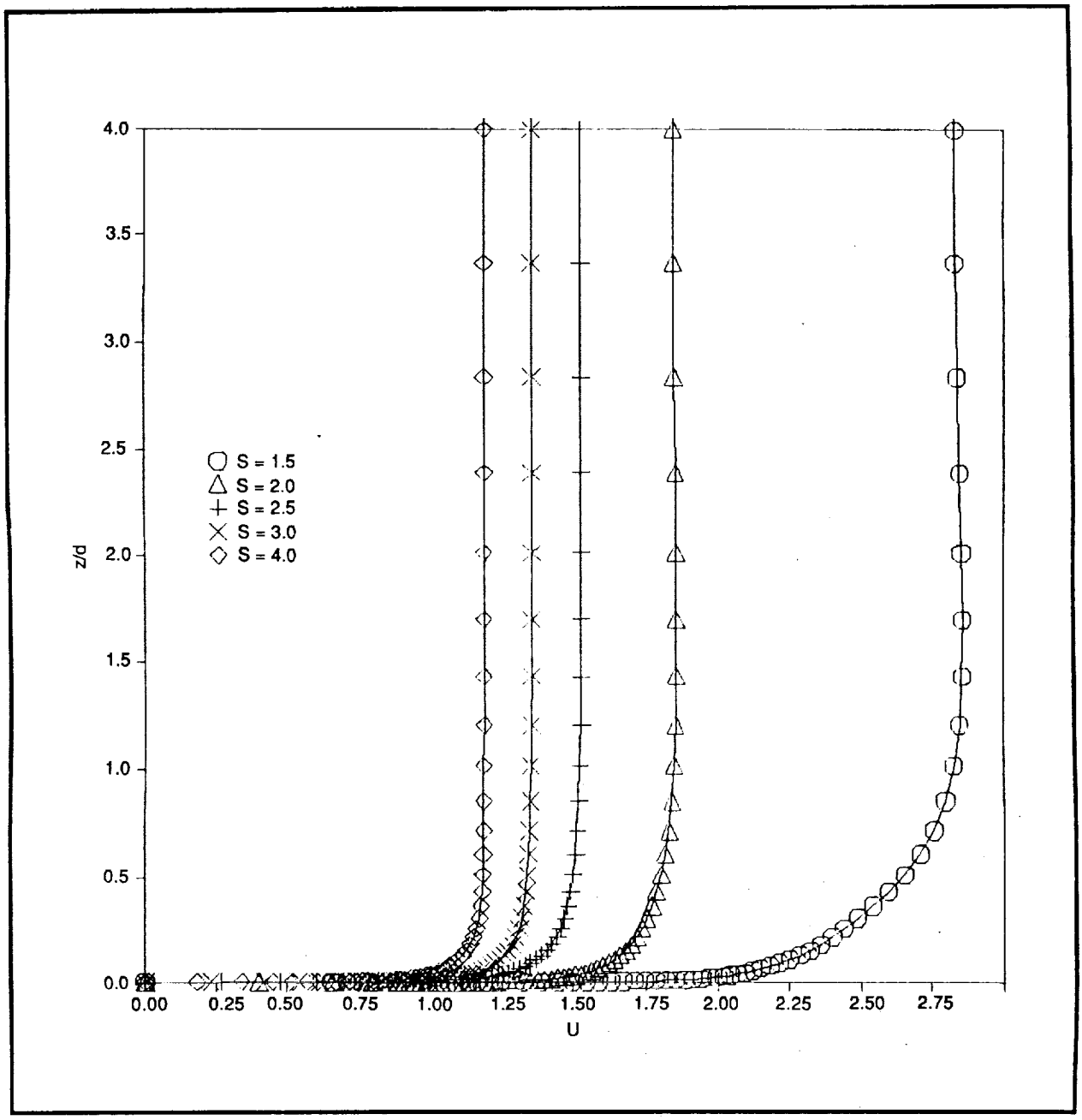

Figure 17 Vertical Variation of Velocity at x/d=0.5, y/s=0.5

Velocity profiles are presented for the five different post spacings. As the post spacing decreases, the maximum gap velocity increases sharply.

The vertical variation of the drag coefficient with height for each of the five post spacings is shown in Fig. 18. The rise in drag coefficient near the flat plate is likely due to the effect of the horseshoe vortex. A similar peak was observed by Kaul et al. (Ref. 15) for laminar flow around a single post. For z/d greater than approximately 2.0, the drag coefficient levels off to a nearly constant value which, except for the most closely spaced post spacings, is generally less than 0.35, the experimental value for a single, two-dimensional cylinder at the Reynolds number of one million (Ref. 16). Although the reason for the low computed drag coefficient is not known for certain, one possible explanation concerns the fact that the computations assume the boundary layer to be turbulent everywhere, with no attempt to model the transition that would actually occur at the post leading edge. Experiments on circular cylinders (Ref. 16) have shown that the addition of roughness elements on the cylinder surface will move the transition point upstream, resulting in a lower value of Cd. This trend is consistent with that observed in the computations, which effectively assume the transition point to be at the post leading edge.

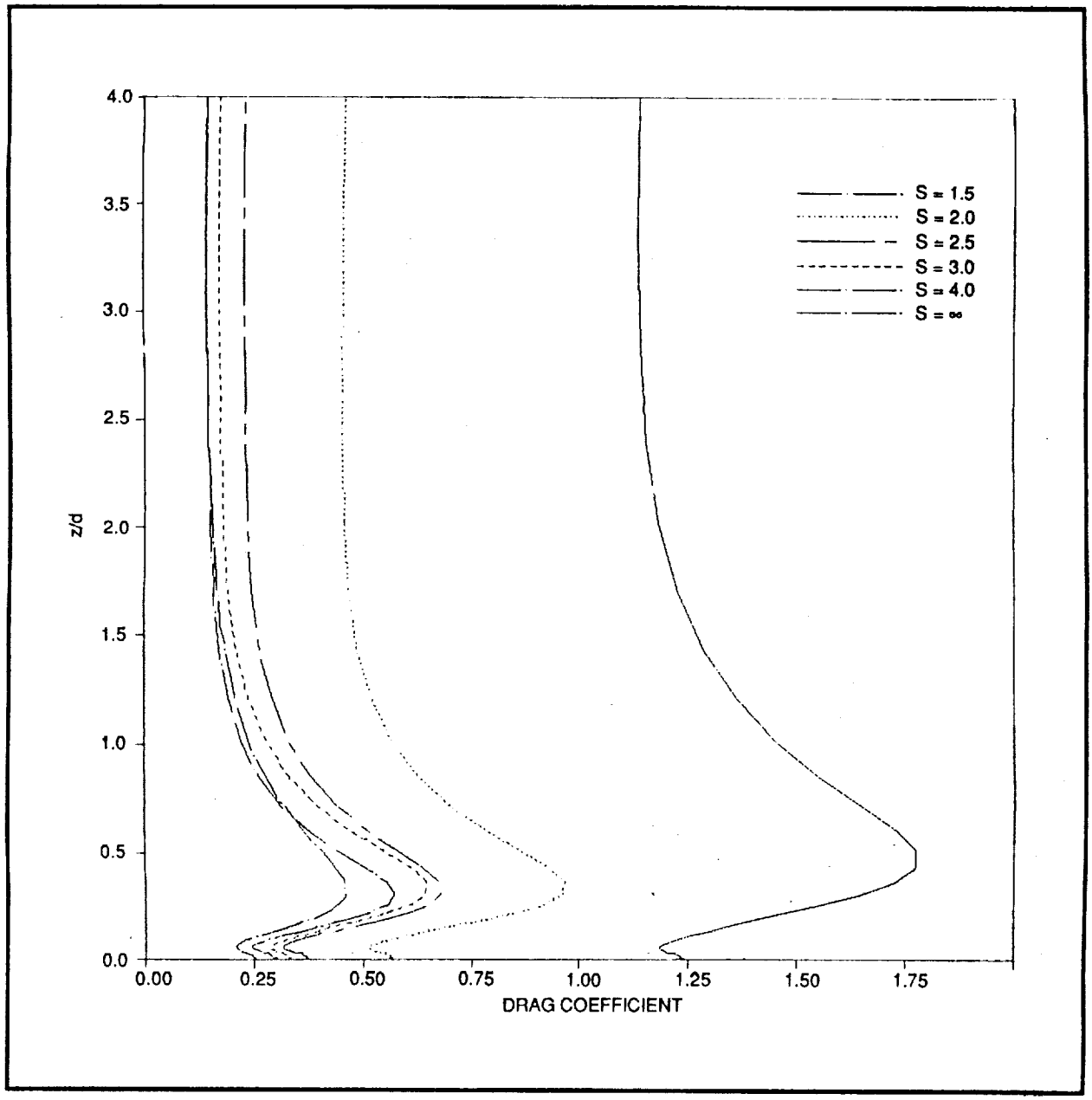

Figure 18 Vertical Variation of Drag Coefficient

4. CONCLUSIONS

This study has examined the turbulent flow around multiple posts using a simple mixing length model to achieve closure. Comparison with the experimental data of Baker (Ref. 6) for a single post on a flat plate revealed a generally good correlation with the size of the horseshoe vortex and pressure distribution upstream of the post.

For the multiple post calculations only one post was modeled, with periodic boundary conditions applied at the side boundaries to simulate an infinite row of posts. The variation of the flowfield parameters with post spacing was investigated by altering the distance between the side boundaries. The computed results showed significant interaction between the horseshoe vortex systems of adjacent posts as the spacing decreased. The total pressure drop across the posts was found to increase sharply with smaller post spacing, due to the increased amounts of separation. The streamwise velocity profiles in the gap between the posts were also analyzed, revealing a progressively less steep velocity gradient near the wall as the post spacing increased. This relationship is believed due to the presence of the horseshoe vortex system. The vertical variation of drag coefficient for the multiple posts was also considered. The computed values of drag coefficient are believed to be generally underpredicted due to the assumption that transition occurs at the post leading edge.

Future work would include the incorporation of a transition routine in the turbulence model, the placement of a second row of posts in the streamwise direction, the effect of the protective plates, and more realistic inflow conditions with an angle of attack.

5. REFERENCES

1. Cerutti, E.A., R. Kinney, and M. Paolino, "Numerical Predictions for Unsteady Viscous Flow Past an Array of Cylinders," Int. J. for Numerical Methods in Fluids, Vol. 6, 1986, pp. 715-31.

2. Antonopoulos, K. A. and A.D. Gosman, "The Prediction of Laminar Inclined Flow Through Tube Banks," Computers & Fluids, Vol. 14, 1986, pp. 171-80.

3. Antonopoulos, K. A., "The Prediction of Turbulent, Inclined Flow in Rod Bundles," Computers & Fluids, Vol. 14, 1986, pp. 361-78.

4. Rogers, S.E., D. Kwak, and U. K. Kaul, "A Numerical Study of Three-Dimensional Incompressible Flow Around Multiple Posts," Conf. Paper No. AIAA-86-0353, AIAA 24th Aerospace Sciences Meeting, Reno, NV, 6-9 January, 1986.

5. Williams, M., "Navier-Stokes Calculation of the Flow Around Simplified LOX Posts Arrays," Conf. Paper No. AIAA-87-0488, AIAA 25th Aerospace Sciences Meeting, Reno, NV, 12-15 January, 1987.

6. Baker, C.J., "The Turbulent Horseshoe Vortex," J. Wind Eng. and Indus. Aerodyn., Vol. 6, 1980, pp. 9-23.

7. Kwak, D., J.L.C. Chang, S.P. Shanks, and S.R. Shakravarthy, "A Three-Dimensional Incompressible Navier-Stokes Flow Solver Using Primitive Variables," AIAA Journal, Vol. 24, 1986, pp. 390-96.

8. Briley, W.R. and H. McDonald, "Solution of the Multidimensional Compressible Navier-Stokes Equations by a Generalized Implicit Method," J. Comp. Physics, Vol. 24, 1977, p. 372.

9. Warming, R.F. and R.M. Beam, "On the Construction and Application of Implicit Factored Schemes for Conservation Laws," Symposium on Computational Fluid Dynamics, SIAM-AMS Proceedings, Vol. 11, 1977.

10. Chorin, A.J., "A Numerical Method for Solving Incompressible Viscous Flow Problems," J. Comp. Physics, Vol. 2, 1987, p. 12.

11. Patankar, S.V., M. Ivanovic, and E.M. Sparrow, "Analysis of Turbulent Flow and Heat Transfer in Internally Finned Tubes and Annuli," J. of Heat Transfer, Vol. 101, 1979, pp. 29-37.

12. Burke, R.W., "Computation of Turbulent, Incompressible Wing-Body Junction Flow," Conf. Paper No. AIAA-89-0279, AIAA 27th Aerospace Sciences Meeting, Reno, NV, 9-12 January, 1989.

13. Dickinson, S.C., "An Experimental Investigation of Appendage-Flat Plate Junction Flow," Vols. 1 and 2, DTNSRDC 86/051 and 86/052, David Taylor Naval Ship Research & Development Center, Bethesda, MD, December 1986.

14. Chang, J.L.C., D. Kwak, S.C. Dao, and R. Rosen, "A Three-Dimensional Incompressible Flow Simulation Method and Its Application to the Space Shuttle Main Engine, Part I - Laminar Flow," Conf. Paper No. AIAA-85-0175, AIAA 23rd Aerospace Sciences Meeting, Reno, NV, 14-17 January 1985.

15. Kaul, U.K., D. Kwak, and C. Wagner, "A Computational Study of Saddle Point Separation and Horseshoe Vortex System," Conf. Paper No. AIAA-85-0182, AIAA 23rd Aerospace Sciences Meeting, Reno, NV, 14-17 January 1985.

16. Schlichting, H., Boundary-Layer Theory, McGraw-Hill, New York, 1968.